

Model Predictive Pulse Pattern Control for the Five-Level Active Neutral Point Clamped Inverter

Nikolaos Oikonomou, *Member, IEEE*, Christof Gutscher, Petros Karamanakos, *Student Member, IEEE*, Frederick Kieferndorf, *Member, IEEE* and Tobias Geyer, *Senior Member, IEEE*

Abstract—In this paper, the recently introduced model predictive pulse pattern control (MP³C) strategy is adapted to the ACS 2000 medium voltage drive of ABB. The drive system consists of a five-level active neutral-point clamped (ANPC-5L) rectifier and inverter and an induction machine. The inverter is fed with offline computed optimized pulse patterns (OPPs) that produce minimum harmonic distortion in the stator windings of the ac machine. An optimal stator flux trajectory is calculated from these OPPs and a trajectory controller tracks it in real-time. In the proposed approach, trajectory tracking is based on model predictive control (MPC): a constrained optimal control problem is formulated and solved in real-time in a computationally efficient manner. An event-based prediction horizon is employed in order to ensure fast tracking of the stator flux trajectory. The advantages of the proposed method are optimal steady-state behavior in terms of harmonic distortion and fast torque response. The method was tested on a medium-voltage ANPC-5L inverter coupled to a general-purpose 1.21-MW induction machine. Experimental results were obtained from this industrial setup and they are presented in this paper to demonstrate the high performance of MP³C.

Index Terms—AC drive, optimized pulse pattern, model predictive control, five-level active neutral point inverter, medium-voltage drive.

I. INTRODUCTION

ABB has recently introduced the ACS 2000 general-purpose medium-voltage (MV) drive to provide speed and torque control in a wide range of applications that include control of industrial fans and pumps [1]. Fig. 1 shows a typical drive configuration including an active rectifier stage, a dc-link and an inverter stage connected to a MV induction machine. This power converter is based on the five-level active neutral-pointed clamped (ANPC-5L) topology [2]. The circuit diagram of one phase leg of the ANPC-5L topology is shown in Fig. 2.

General-purpose drives can be used to control standard direct-on-line (DOL) induction machines, which are characterized by a low value of leakage inductance x_{σ} , usually in the range of 0.18 p.u.. In the inverter-controlled configuration of Fig. 1, a DOL machine is fed with pulse width modulated (PWM) voltage waveforms. The minimization of the harmonic

distortion of the stator currents is of special interest and is a particularly challenging task owing to the low value of x_{σ} .

Increasing the switching frequency of the semiconductor switches would allow the minimization of the distortion of the output voltage waveforms and of the machine currents. However, in MV configurations such as that of Fig. 1, the switching frequency cannot be increased beyond a few hundred Hertz per semiconductor because of thermal constraints imposed by the IGBT technology of the semiconductor devices. A further limiting factor is the number of additional switching transitions that are required to control the neutral point potential of the dc-link and the voltages of the phase capacitors of the ANPC-5L around their reference values. The neutral point (N) of the shared dc-link and the phase capacitor (C_{ph}) of one phase leg of the ANPC-5L are shown in Fig. 2. Waveforms of the neutral point potential and of one phase capacitor voltage are shown in steady-state operation in Fig. 3. The additional pulses that are necessary to control the neutral point potential and the phase capacitor voltages make use of the inherent voltage redundancies of the ANPC-5L. A method for establishing control of the inverter-internal voltages is presented in [3].

In MV drives, it is crucial to select the PWM method such that the harmonic distortion of the currents in the machine windings is low. A further requirement is to operate the semiconductor devices of the power converter at low switching frequencies. Conventional PWM methods, such as space vector modulation (SVM), can achieve these two conflicting objectives only in a limited region of the modulation range, typically below 50% of the rated voltage of the inverter [4]. In the upper modulation range, SVM is not suited to achieve low current harmonics.

N. Oikonomou, F. Kieferndorf and T. Geyer are with ABB Corporate Research, Baden-Dättwil, Switzerland; e-mails: nikolaos.oikonomou@ch.abb.com, frederick.kieferndorf@ch.abb.com and t.geyer@ieee.org

C. Gutscher is with ABB Switzerland LTD., Medium Voltage Drives, Turgi, Switzerland; e-mail: christof.gutscher@ch.abb.com

P. Karamanakos is with the Department of Electrical and Computer Engineering, National Technical University of Athens, Athens, Greece; e-mail: petkar@central.ntua.gr

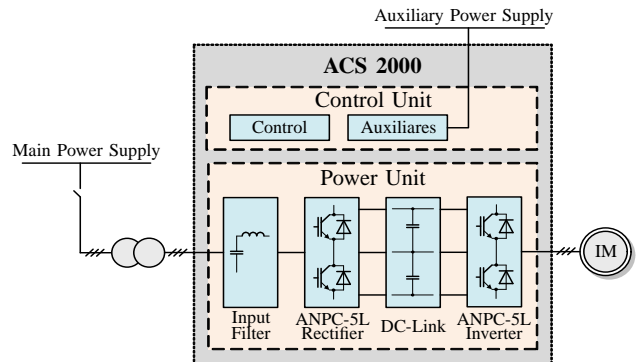


Fig. 1. Configuration of the ACS 2000 drive system from ABB.

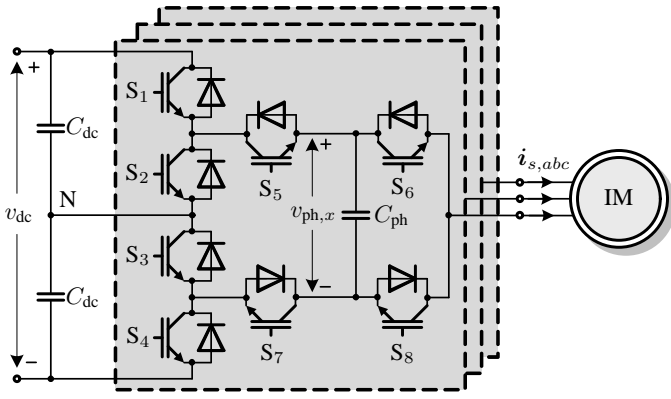


Fig. 2. Circuit diagram of the five-level active neutral point clamped (ANPC) voltage source inverter driving an induction machine (IM).

A more suitable solution is offered through the use of synchronous optimal modulation. Offline-calculated optimal pulse patterns (OPPs) [5]–[7] can achieve values of total demand distortion (TDD) of the machine current which are less than 5% of the rated current in the complete linear range of the modulation index m . Individual current harmonics of non-triplen order (5th, 7th, 11th, 13th, ...) are reduced and interharmonic components are eliminated [4].

The use of OPPs in a closed-loop control system, however, is difficult in practice because discontinuities in the switching angles can introduce harmonic excursions [8]. Fig. 4(c) shows the switching angles of OPPs of pulse number $d = 5$ per quarter wave plotted over the modulation index and a high number of discontinuities in the switching angles can be observed. With the motor drive in operation, only a narrow band of the switching angles of a given pulse number d is used. The selection of the band is such that the switching frequency $f_{sw} = df_1$, where f_1 is the fundamental frequency, does not exceed a preset limit. As f_1 increases, the pulse number d decreases, e.g. from $d = 5$ to $d = 4$. Such a transition between neighboring pulse patterns can also introduce harmonic excursions in the machine current. A solution is offered through control by trajectory tracking [8] which can maintain the optimal volt-seconds balance of OPPs under quasi steady-

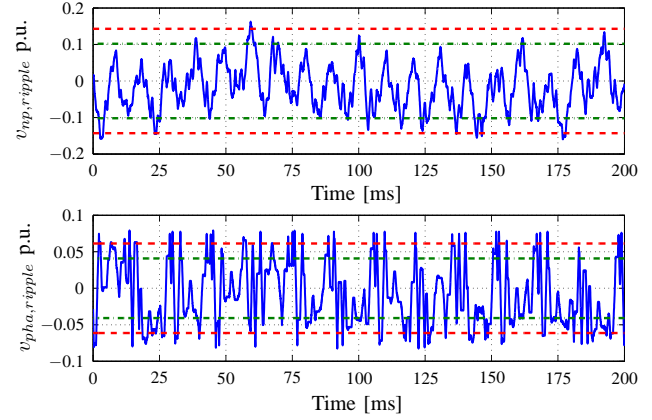
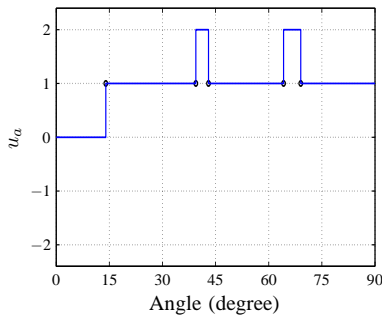


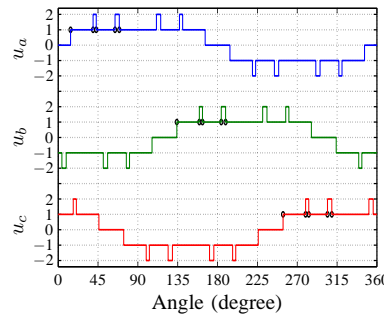
Fig. 3. Inverter-internal voltage waveforms of the ANPC-5L recorded at 32 Hz and 42% load; *Top*: neutral point potential, *Bottom*: ac ripple of phase capacitor voltage. Both values are shown in p.u..

state conditions in both cases where harmonic excursions can occur. Establishing control by trajectory tracking of the stator flux trajectory is the preferred method since it does not require estimating the leakage inductance of the machine in real-time [8]. However, state-of-the art flux trajectory tracking requires real-time estimation of the fundamental of the stator flux trajectory *separately* from the flux harmonics [9].

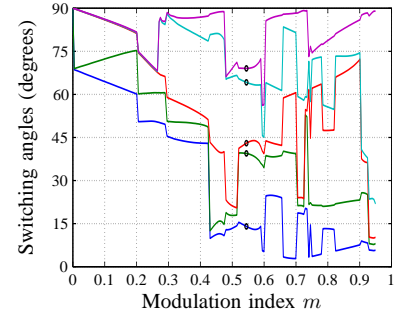
A more recent solution that addresses this problem is model predictive pulse pattern control (MP³C) [10] where the stator flux control problem is addressed from the perspective of model predictive control (MPC) [11], [12]. MPC has recently been gaining popularity in the field of power electronics [13]–[18] because of its advantages in terms of straightforward implementation and the explicit inclusion of constraints coupled with the more powerful controllers available in modern converters. MPC is based on a mathematical model of the system and operates by minimizing an objective function in real-time. In this work, the objective function to be minimized is chosen as the deviation of the stator flux vector from its optimal trajectory within a time prediction horizon of finite length.



(a) Optimized pulse pattern; $d = 5$, $m = 0.55$, phase a .



(b) Three-phase optimized pulse pattern; $d = 5$, $m = 0.55$.



(c) Optimized switching angles; $d = 5$.

Fig. 4. Five-level optimized pulse pattern $\mathcal{P}(m, d)$ with $d = 5$ switching angles per quarter wave. The switching angles at $m = 0.55$ are indicated by black circles.

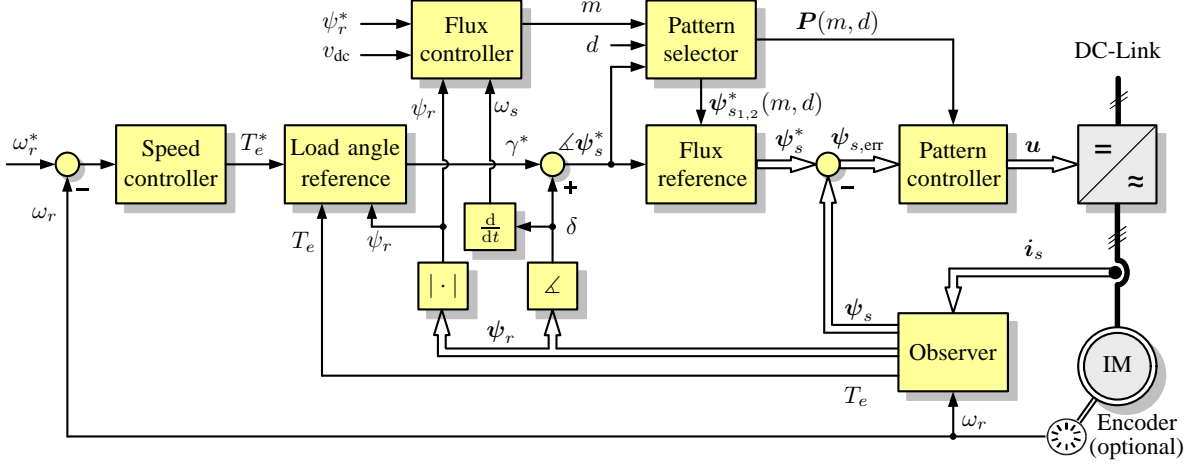


Fig. 5. Block diagram of the model predictive pulse pattern controller (MP³C).

TABLE I
PHASE VOLTAGES OF THE ANPC-5L INVERTER AND THE
CORRESPONDING SWITCHING COMBINATIONS

$v_{ph,x}$	Switching Combination							
	S_1	S_2	S_3	S_4	S_5	S_6	S_7	S_8
$v_{dc}/2 = v_{dc,up}$	1	0	1	0	1	1	0	0
$v_{dc}/4 = v_{dc,up} - v_{ph,x}$	1	0	1	0	1	0	0	1
$v_{dc}/4 = v_{ph,x}$	1	0	1	0	0	1	1	0
0	1	0	1	0	0	0	1	1
0	0	1	0	1	1	1	0	0
$-v_{dc}/4 = -v_{ph,x}$	0	1	0	1	1	0	0	1
$-v_{dc}/4 = -v_{dc,lo} + v_{ph,x}$	0	1	0	1	0	1	1	0
$-v_{dc}/2 = -v_{dc,lo}$	0	1	0	1	0	0	1	1

The present paper is an *industrial* implementation of MP³C, tailored to the requirements of the ANPC-5L MV drive. The underlying optimization problem is solved in real-time in a computationally-efficient manner to provide the sequence of switching angles (the control input) that allows the operation with OPPs in quasi steady-state. The deadbeat implementation of MP³C in [10] is refined to achieve high dynamic performance in closed loop despite computational limitations on the length of the prediction horizon.

This paper is organized as follows. The ANPC-5L topology is summarized in Section II. In Section III the principle of the stator flux trajectory tracking is presented. Section IV describes the proposed control algorithm in detail including the derivation of the optimal flux trajectory from the OPPs and the formulation of the optimization problem. In Section V the performance of the controller is demonstrated in an industrial ANPC-5L. Finally, in Section VI conclusions are drawn.

II. FIVE-LEVEL ACTIVE NEUTRAL POINT CLAMPED INVERTER

The ANPC-3L inverter produces three different phase to neutral voltage levels $\{-v_{dc}/2, 0, +v_{dc}/2\}$, where v_{dc} is the total dc-link voltage. The ANPC-5L phase leg is derived from the ANPC-3L phase leg by inserting a phase capacitor,

C_{ph} , between the series connected output switches S_5/S_6 and S_7/S_8 [1] as shown in Fig. 2. By choosing the nominal voltage of the phase capacitors to be $v_{dc}/4$, five different, evenly spaced phase to neutral voltage levels, $v_{ph,x}$, with $x \in \{a, b, c\}$ can be produced. The phase capacitor voltage can be added or subtracted from the neutral point potential as well as subtracted from $v_{dc,up}$ or added to $v_{dc,lo}$. As a result, the ANPC-5L inverter produces the following phase to neutral voltage levels $\{-v_{dc}/2, -v_{dc}/4, 0, +v_{dc}/4, +v_{dc}/2\}$.

The phase leg of the ANPC-5L inverter has eight allowed switching states, two of which produce unique output voltages: $\{-v_{dc}/2, +v_{dc}/2\}$. The remaining three voltage levels $\{-v_{dc}/4, 0, +v_{dc}/4\}$ have two associated switching states each. This is shown in more detail in Table I, where all the allowed switching combinations are shown with the resulting voltages. As previously mentioned, these redundancies can be effectively exploited to control the neutral point and phase capacitor voltages, as described in [3].

III. PRINCIPLE OF STATOR FLUX TRAJECTORY TRACKING

Optimized pulse patterns are calculated offline and stored in a look-up table for use in real-time operation, [5]–[7]. The entries of the look-up table are read out in real-time by making use of the modulation index m and the pulse number d as inputs as shown in the block diagram of Fig. 5. The pulse number d is selected relative to the fundamental frequency of the drive system, f_1 , with the following relation: $d = \text{floor}(f_{sw}/f_1)$, where f_{sw} is the switching frequency of the semiconductor devices. The selection $f_{sw} = f_{sw,max}$ ensures that the maximum value of the switching frequency is not exceeded. The modulation index m is adjusted through a conventional linear controller of the rotor flux amplitude ψ_r of the ac machine as seen in Fig. 5. The output of the flux controller block in this figure is the modulation index $m = m_{FF} + m_{PI}$. The first term of this sum adjusts the voltage to be in proportion to the stator frequency, $m_{FF} = (v_{dc,nom}/v_{dc})\omega_s\psi_r$, where $v_{dc,nom}$ is the nominal value of the dc-link voltage. The second term of the sum is the

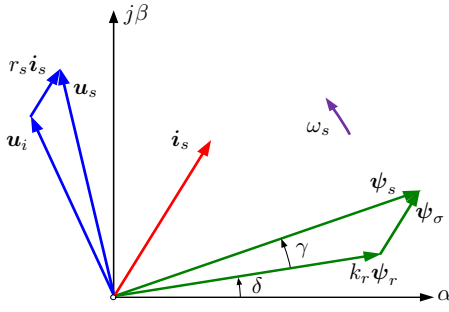


Fig. 6. Diagram of voltage, current and flux linkage space vectors in an induction motor.

output of a PI controller that compensates for the long-term error in the amplitude of the rotor flux $\psi_r^* - \psi_r$.

The pair (m, d) defines the operating point of the drive system through the optimized pulse sequence $P(m, d)$. An example of an optimized three-phase pattern which is valid for $m = 0.55$ and $d = 5$ is shown in Fig. 4(b). When fed to the electrical machine through the inverter without further modification, the optimized pulse pattern generates three-phase voltages in the stator windings whose sinusoidal spatial distributions are described by the respective voltage space vector, \mathbf{u}_s , shown in the vector diagram of Fig. 6. The electromagnetic field in the stator winding is described by the stator flux space vector

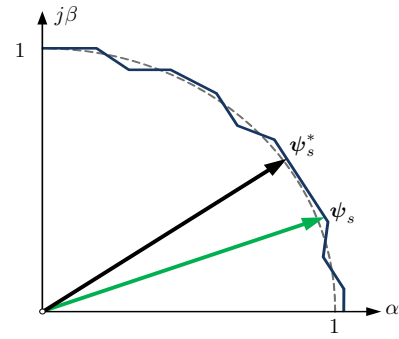
$$\psi_s(t) = \psi_s(0) + \int_0^t \mathbf{u}_s(\tau) d\tau, \quad (1)$$

also shown in Fig. 6. Assuming operation at steady-state and an inverter of ideal switching behavior, the stator flux space vector would track an optimized reference flux trajectory. An example is shown in Fig. 7(a) over one quarter of the fundamental period. Under ideal conditions, the voltage in the stator windings would match exactly the optimized pulse pattern waveforms and the harmonic distortion of the stator currents would be equal to its offline-calculated value.

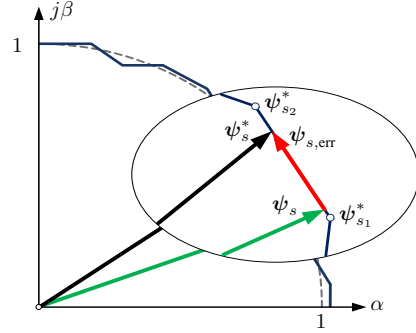
However, the behavior of the drive system is non-ideal owing to non-linear effects of the inverter. These include instantaneous deviations of the neutral point potential from zero, deviations of the phase capacitor voltages from their reference values and non-idealities of the inverter system such as the dead-time effect [19]. The instantaneous excursions of the inverter-internal voltage waveforms from their reference values, shown in Fig. 3, are manifested as deviations of the flux space vector from its reference trajectory. The result is increased harmonic content in the stator currents of the machine despite the utilization of optimized pulse patterns. In addition to this, deviations from the reference flux trajectory occur when the drive operates dynamically, e.g. during step changes of the load torque or in the event of a ride-through condition. Such errors have to be compensated very quickly to avoid a trip due to overcurrent conditions in the drive system.

Any deviation of the stator flux space vector ψ_s from its reference trajectory ψ_s^* can be described by the flux error space vector

$$\psi_{s,\text{err}} = \psi_s^* - \psi_s. \quad (2)$$



(a) Flux linkage space vector ψ_s and reference flux trajectory ψ_s^* .



(b) The flux error vector $\psi_{s,\text{err}}$ in detail.

Fig. 7. The reference flux vector ψ_s^* is calculated in real-time by linear interpolation between the pre-stored values ψ_{s1}^* and ψ_{s2}^* .

Control through stator flux trajectory tracking aims at compensating the stator flux error $\psi_{s,\text{err}}$ in real-time by modifying the volt-second area of the original, offline-calculate pulse pattern $P(m, d)$, which is valid only for an ideal system operated at steady-state [4]. Eliminating the flux error allows the drive system to maintain its operating point (m, d) while generating currents of minimum harmonic distortion in the stator windings of the machine. This is due to the linear relationship between flux and current harmonics: optimization of the stator flux trajectory amounts to optimal current waveforms in the machine windings [4].

Moreover, stator flux trajectory tracking also enables torque control. This is explained with reference to the vector diagram in Fig. 6 that shows the space vectors of the stator and rotor flux linkages describing the electrical subsystem of the ac machine [20]. For reasons of completeness, Fig. 6 shows the space vectors of further electrical quantities of the ac machine in motoring operation. The flux leakage is the difference between stator and rotor flux ($\psi_\sigma = \psi_s - k_r \psi_r$) and the stator voltage is the sum of the induced voltage and the voltage drop on the stator resistance ($\mathbf{u}_s = \mathbf{u}_i + r_s \mathbf{i}_s$), where \mathbf{i}_s is the stator current. The amplitude of the flux vectors and their angular displacement γ determine the magnitude of the torque T_e generated at the rotor shaft of the machine by the interaction of the electromagnetic fields of the stator and rotor windings through the air gap,

$$T_e = k_r \psi_r \psi_s \sin \gamma, \quad (3)$$

where k_r is the rotor coupling factor. Assuming knowledge of the quantities in (3) and a given reference torque value T_e^* , the problem of torque control becomes the adjustment of the stator flux space vector ψ_s to coincide in intensity and angular displacement with the reference flux ψ_s^* at any given time instant t .

The procedure is explained with reference to the block diagram in Fig. 5 where the torque reference T_e^* is the output of a conventional speed controller. An observer of the state variables that describe the electrical machine is fed by the measured stator current i_s and the angular velocity of the rotor ω_r [21]. The observer estimates the complex state variables ψ_s and ψ_r , and the electromagnetic torque T_e (3). The reference amplitude of the rotor flux space vector ψ_r^* is held constant in the base speed range, as shown in Fig. 5. The angular displacement δ of the rotor flux space vector ψ_r with reference to the real axis of the stationary coordinate system (Fig. 6) is estimated in real-time as $\delta = \arg(\psi_r)$.

With the present state of the electrical machine estimated by the observer, the next task is to determine the phase angle of the reference stator flux ψ_s^* that corresponds to the reference torque value T_e^* . When the machine is fully magnetized, the magnitude of the reference stator flux vector is equal to 1 p.u.. Then, for a constant value of the rotor flux magnitude and a given torque reference, the desired angle between the stator and rotor flux vectors is calculated as

$$\gamma^* = \sin^{-1} \left(\frac{T_e^*}{k_r \psi_r \psi_s^*} \right). \quad (4)$$

The reference stator flux trajectory is then obtained by integrating the chosen three-phase pulse pattern where the reference stator flux angle,

$$\angle \psi_s^* = \gamma^* + \delta, \quad (5)$$

is the upper limit of the integral in (1). With the reference flux ψ_s^* available, the calculation (2) is straight-forward. Contrary to state-of-the-art methods [9], it is not required to estimate the fundamental component of the stator flux error separately of its harmonic component. With this procedure, the torque and flux control problem of the drive system can be resolved by compensating the error vector $\psi_{s,\text{err}}$. The details of the implementation of trajectory tracking for the specific case of the ANPC-5L drive system are explained in the next section.

IV. MODEL PREDICTIVE PULSE PATTERN CONTROL (MP³C) FOR THE ANPC-5L INVERTER

The control objective of the proposed method is to compensate the flux error in real-time by modifying the pre-calculated switching instants of the OPPs. The flux error compensation must be achieved as quickly as possible while simultaneously maintaining low distortion in the machine currents in the complete modulation index range.

In a first step, the reference flux trajectory is calculated offline by integrating the respective OPPs according to (1) over 90° of the fundamental voltage waveform. The result of this integration procedure is a set of corners points (see

Fig. 7b) with each corner point corresponding to a switching transition in the OPP. These corner points are stored in a look-up table along with the OPP patterns. Thus, the following information is readily available at each operating point (m, d) in the discretized modulation range:

- i) The d switching angles of the OPP. Owing to the quarter-wave symmetry of the optimized pulse sequences (see Fig. 4) only the angles over the first 90° of the fundamental period need to be stored in the look-up table.
- ii) The respective switching states of the OPP over 90° of the fundamental period.
- iii) The corner point component values $\psi_{s,\alpha}^*$ and $\psi_{s,\beta}^*$ of the reference flux vector referred to in stationary coordinates, i.e. $\psi_s^* = \psi_{s,\alpha}^* + j\psi_{s,\beta}^*$. The reference flux trajectory exhibits a 30° symmetry, thus, only the value pairs $(\psi_{s,\alpha}^*, \psi_{s,\beta}^*)$ over this range are stored in the look-up table.

Storing the reference flux coordinates for the corner points in the look-up table—rather than calculating them in real-time through (1)—greatly reduces the complexity of mathematical operations that need to be performed in real-time

Given the operating point (m, d) , the corresponding flux reference corner points are compared to the angular position (5), referring to Fig. 5. The components of the reference flux vectors ψ_{s1}^* and ψ_{s2}^* that are adjacent to the desired reference flux vector are retrieved from the look-up table, noted as $\psi_{s1,2}^*(m, d)$ in Fig. 5. Next, a linear interpolation is performed between ψ_{s1}^* and ψ_{s2}^* (see Fig. 7b) to determine the flux reference vector ψ_s^* , a process that requires very few mathematical calculations.

The correction of the flux error $\psi_{s,\text{err}}$ is achieved by modifying in real-time the pre-stored switching instants of the OPPs. The volt-second area that the PWM sequence of each phase contributes to the flux is either increased or decreased depending on the direction of the needed modification and on the switching transition. An example is shown in Fig. 8(a) where a modification of the switching instants of two phases must be made. The volt-second area in phase a is reduced by Δt_a and the volt-second area in phase b is increased by Δt_b . The modifications, Δt_a and Δt_b , are made such that the respective a - and b -components of the stator flux error, $\psi_{s,\text{err}}$, are minimized. In general, modifying the value of a pre-calculated (nominal) switching instant t_x^* , $x \in \{a, b, c\}$, by a time interval Δt_x results in a modified switching instant $t_x = t_x^* + \Delta t_x$. The volt-second contribution of phase x to the flux correction is:

$$\Delta \psi_{s,x}(\Delta t_x) = -\frac{v_{\text{dc}}}{2} \Delta u_x \Delta t_x, \quad (6)$$

where $\Delta u_x \in \{-1, +1\}$ is the direction of the switching transition and v_{dc} is the total voltage across the two dc-link capacitors C_{dc} . Note that the normalized voltage states u_x of the ANPC-5L inverter are $u_x \in \{-2, -1, 0, +1, +2\}$. Hence, when the next voltage state is larger than the current one, the direction of the transition is $\Delta u_x = +1$. Accordingly, when it is lower, it is $\Delta u_x = -1$.

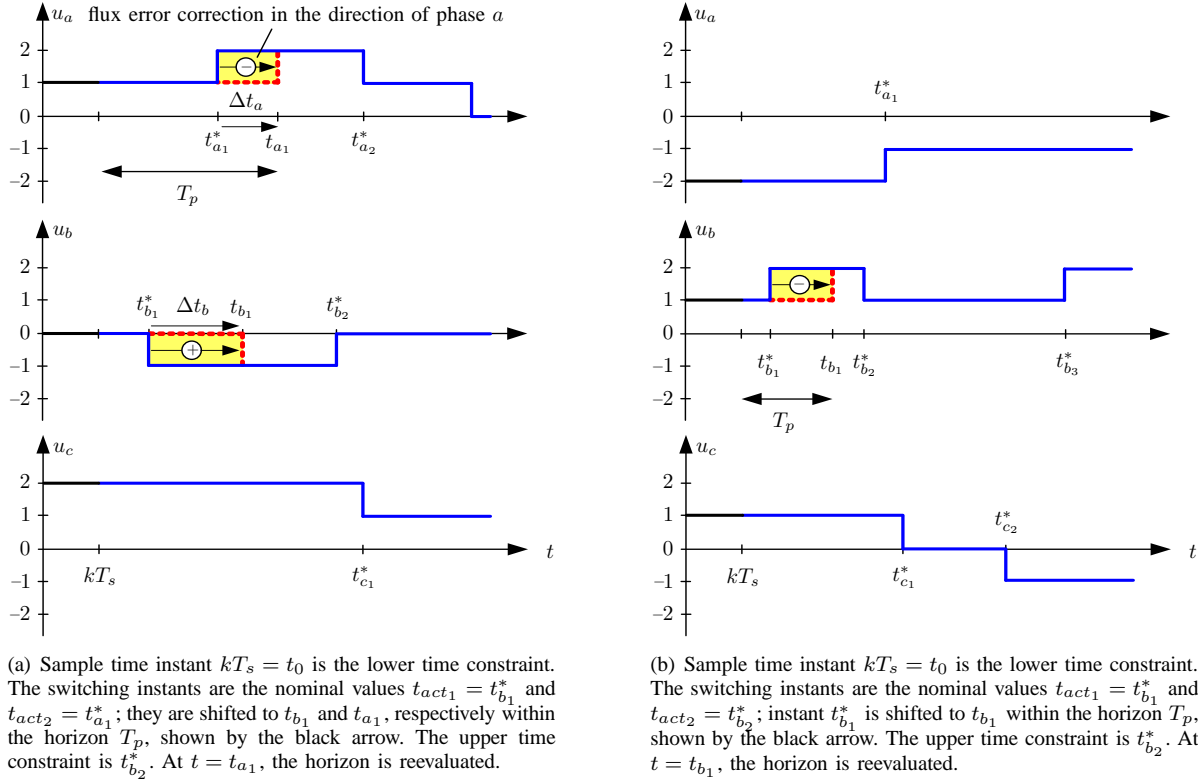


Fig. 8. MP³C is activated at sample time instant kT_s and it modifies pre-calculated switching instants of a three-phase, five-level pulse pattern.

In a next step, the formulated objective function is minimized in real-time:

$$J(\Delta t) = |\psi_{s,\text{corr}}(\Delta t) - \psi_{s,\text{err}}|, \quad (7)$$

where $\psi_{s,\text{corr}}(\Delta t)$ is the correction of the stator flux given by

$$\psi_{s,\text{corr}}(\Delta t) = -\frac{v_{\text{dc}}}{2} \mathbf{K} \begin{bmatrix} \Delta u_a \Delta t_a \\ \Delta u_b \Delta t_b \\ \Delta u_c \Delta t_c \end{bmatrix}, \quad (8)$$

with the matrix \mathbf{K} being

$$\mathbf{K} = \frac{2}{3} \begin{bmatrix} 1 & -\frac{1}{2} & -\frac{1}{2} \\ 0 & \frac{\sqrt{3}}{2} & -\frac{\sqrt{3}}{2} \end{bmatrix}. \quad (9)$$

Furthermore, $\Delta t = [\Delta t_{a1} \ \Delta t_{a2} \ \dots \ \Delta t_{b1} \ \dots \ \Delta t_{c1} \ \dots]^T$, is the vector of the switching instant modifications, i.e. the manipulated variables. Function (7) is the amplitude of the residual flux error at the end of a prediction horizon of finite length T_p . By modifying the switching instants of the OPP within this horizon, the flux error is minimized and—if possible—eliminated. However, in contrast to the vast majority of the introduced MPC approaches in power electronics the length of the prediction horizon is not fixed, it is rather a function of the nominal and modified switching instants of the phases that commute within the horizon and the horizon is computed in real-time. The calculation of the prediction horizon T_p is outlined next.

Starting from the sampling instant $t_0 = kT_s$, the two future nominal switching instants, t_{act1} and t_{act2} , which are closest to t_0 are identified. The following two cases are considered:

- If the two switching instants that follow t_0 occur in different phases, the flux error vector is projected onto these two phases. In this case, two active phases, i.e. two degrees of freedom, are available to compensate the error: $\{a, b\}$, $\{b, c\}$ or $\{c, a\}$. In Fig. 8(a), the two active switching instants $t_{act1} = t_{b1}^*$ and $t_{act2} = t_{a1}^*$ are in phases b and a , respectively.
- If both switching instants t_{act1} and t_{act2} that follow t_0 occur in the same phase, then switching instants in a single active phase, a , b or c , are available to reduce the flux error. In Fig. 8(b), both active switching instants $t_{act1} = t_{b1}^*$ and $t_{act2} = t_{b2}^*$ are in phase b .

The length of the horizon is equal to the maximum difference between the initial sample instant t_0 and the nominal or modified switching instants (Fig. 8), i.e.

$$T_p = \max \{t_x^* - t_0, t_x - t_0\}. \quad (10)$$

Based on (10) an *event*-based horizon is defined. The selection of the prediction horizon is key to the application-oriented implementation of MP³C that is outlined here. By restricting the length of the horizon to include only two switching events, the computational effort is significantly reduced relative to an unconstrained prediction horizon, but sufficiently long to effectively correct the flux error. This trade-off makes the

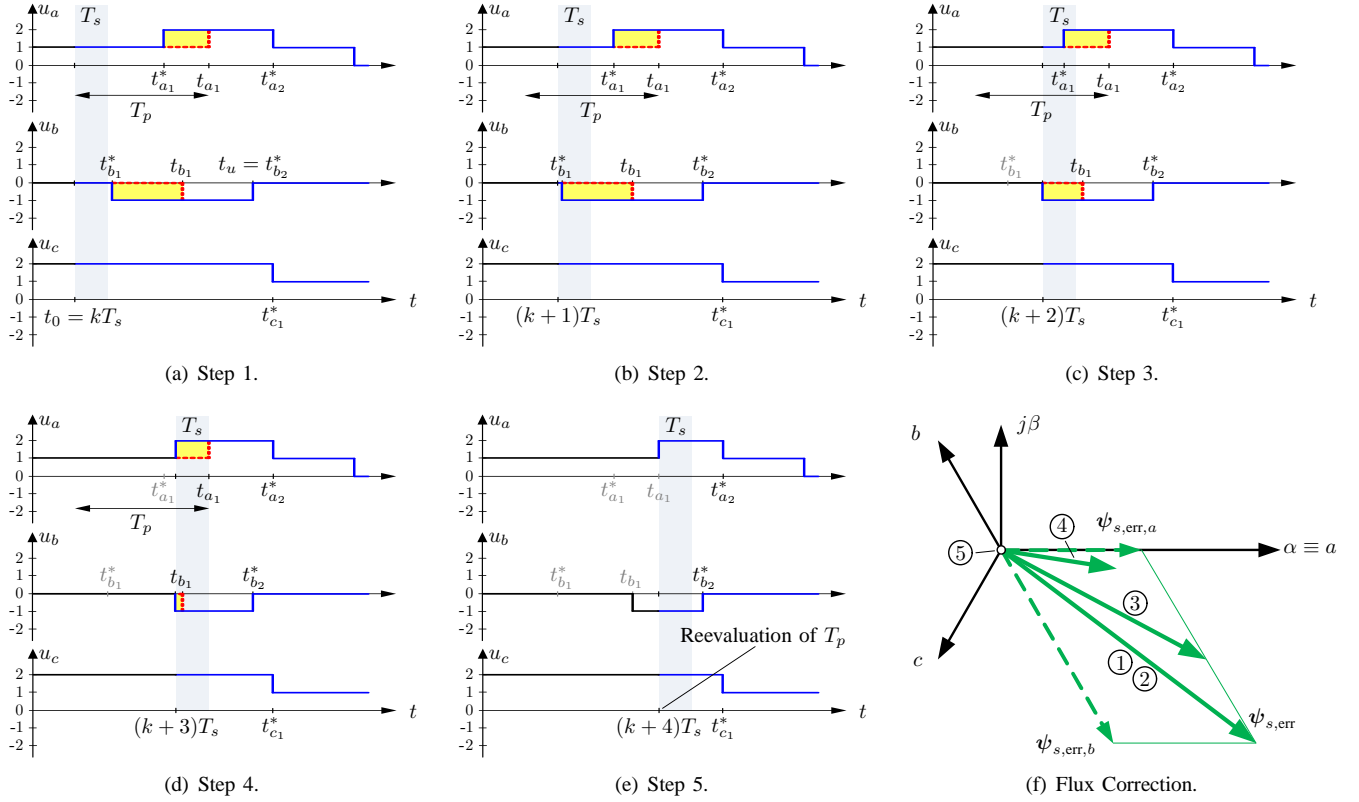


Fig. 9. Example of MP³C compensating flux error $\psi_{s,\text{err}}$ within four sampling intervals $4T_s$. The circled numbers in (f) correspond to the flux error compensation steps shown in (a)–(e).

implementation of MP³C on a standard microprocessor or a field-programmable gate array (FPGA) device possible. In practice, the time horizon is separated into equal sampling intervals of fixed length, $T_s = 25 \mu\text{s}$, based on the execution sampling interval of MP³C. With each iteration of MP³C the horizon is reduced by T_s . When the entire horizon has been scanned, a new prediction horizon T_p is evaluated according to (10) and the flux error correction procedure is repeated.

A further practical issue that determines the length of the prediction horizon is associated with the interaction of the controlling microprocessor or FPGA and an external Flash hardware device where all the offline calculated data are stored. These data, i.e. switching instants, values of switching states and reference flux coordinates, must be read out from the Flash memory at the beginning of every sampling interval T_s . The data transfer takes a fraction of the sampling interval, $T_{\text{int}} \ll T_s$. This imposes a restriction on the maximum length of the prediction horizon T_p .

Before the optimization problem is formulated, upper and lower time constraints must be imposed on the allowed time modification of switching instants. The lower time constraint is equal to the sample time instant t_0 , while the upper time constraint depends on the location of the nominal values of the active switching instants. To be more specific:

- If the active switching instants $t_{\text{act}1}$ and $t_{\text{act}2}$ occur in different phases, e.g. Fig. 8(a), then the upper time constraint is equal to the first nominal (pre-calculated)

switching instant that follows both $t_{\text{act}1}$ and $t_{\text{act}2}$, regardless of which phase it belongs to. In the case of Fig. 8(a), where the active switching instants are $t_{\text{act}1} = t_{b1}^*$ and $t_{\text{act}2} = t_{a1}^*$, the upper time constraint is the switching instant t_{b2}^* , but it could also be t_{c1}^* if it occurred first.

- If both active switching instants $t_{\text{act}1}$ and $t_{\text{act}2}$ occur in the same phase, e.g. Fig. 8(b), then the upper time constraint is equal to the nominal (pre-calculated) switching instant $t_{\text{act}2}$. In the case of Fig. 8(b), where the active switching instants are $t_{\text{act}1} = t_{b1}^*$ and $t_{\text{act}2} = t_{b2}^*$, the upper time constraint is equal to the instant t_{b2}^* .

To generalize, the time constraints are calculated as

$$t_0 \leq t_x \leq \min \{ \mathcal{T}_1 \cup \mathcal{T}_2 \}. \quad (11)$$

In (11) the set \mathcal{T}_1 is defined as $\mathcal{T}_1 = \{ t_x^* \mid t_x^* = t_{x_2}^* \}$, where $t_{x_2}^*$ is the second switching instant of the active phase/s that follow t_0 and the set \mathcal{T}_2 is defined as $\mathcal{T}_2 = \{ t_x^* \mid t_x^* = \bar{t}_{x_1}^* \}$, where $\bar{t}_{x_1}^*$ is the first switching instant of the non-active phase/s.

By taking the objective function (7), the prediction horizon (10) and the linear time constraints (11) into account the following optimization problem is formulated:

$$\begin{aligned} & \text{minimize} && J(k) \text{ over } T_p \\ & \text{subject to} && \text{eq. (11)}. \end{aligned} \quad (12)$$

This optimization problem is solved within each sampling interval T_s yielding a sequence of optimal control inputs



Fig. 10. The ACS 2000 MV drive from ABB.

over the horizon. To solve (12), the flux error vector is projected onto the active phases and the corresponding flux error components are calculated. The component of the flux error on each of the active phases determines the necessary modification of the nominal switching instants of the corresponding phases, (6). The modified switching instants are the optimal control inputs over the horizon. In accordance with the receding horizon policy [11], [12], the *first* control input of this sequence is applied at the end of the first sampling interval, then the length of the horizon is decreased by T_s and the procedure is repeated. When the whole horizon has been scanned, the length of the new prediction horizon T_p is reevaluated together with the new upper and lower constraints, as described above.

Fig. 9 shows a step-by-step example of the flux error correction. The goal is to compensate the flux error $\psi_{s, \text{err}}$ shown as bold solid lines in Fig. 9(f). In Fig. 9(a), the length of the prediction horizon T_p and the lower and upper time constraints, $t_0 = kT_s$ and $t_u = t_{b_2}^*$, respectively, are determined. Also the required time modifications $\Delta t_a = -(t_{a_1}^* - t_{a_1})$ and $\Delta t_b = -(t_{b_1}^* - t_{b_1})$ are calculated within the first sampling interval T_s . The flux correction starts taking effect after the sample instant $(k+1)T_s$ in Fig. 9(b) and the error is fully compensated between $(k+3)T_s$ (Fig. 9(d)) and $(k+4)T_s$ (Fig. 9(e)). In this example, only four sampling intervals elapse between the prediction of the required compensation action, Fig. 9(a) and its successful realization, Fig. 9(d). The new prediction horizon T_p is determined in Fig. 9(e).

V. PERFORMANCE EVALUATION

The proposed MP³C method was tested in the MV laboratory. The test setup consisted of a 1 MVA ACS 2000 MV drive from ABB, Fig. 10, coupled to a 6-kV, 137-A induction machine with a constant mechanical load. Important parameters of the electrical machine are listed in Table II.

TABLE II
PARAMETERS OF MEDIUM-VOLTAGE INDUCTION MACHINE

Rated power	1.21 MW
Rated phase-to-phase voltage (V_{rat})	6 kV rms
Rated phase current (I_{rat})	137 A rms
Rated power factor	0.85
Rated stator frequency (f_{rat})	50 Hz
Rated angular velocity	1488 rpm
Stator resistance	203 m Ω 0.006 p.u.
Rotor resistance	158 m Ω 0.005 p.u.
Main inductance	330 mH 2.96 p.u.
Total leakage inductance	20 mH 0.179 p.u.

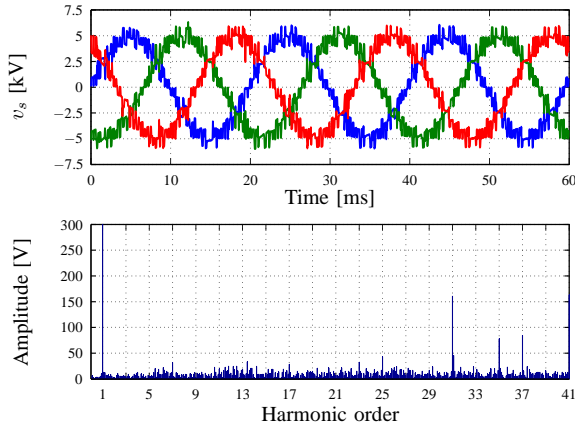
TABLE III
PARAMETERS OF FIVE-LEVEL MEDIUM-VOLTAGE POWER CONVERTER

Rated apparent power	1.14 MVA
Rated phase-to-phase voltage	6.6 kV rms
DC-link voltage	9.8 kV
Rated phase current	100 A rms
Rated frequency	50 Hz

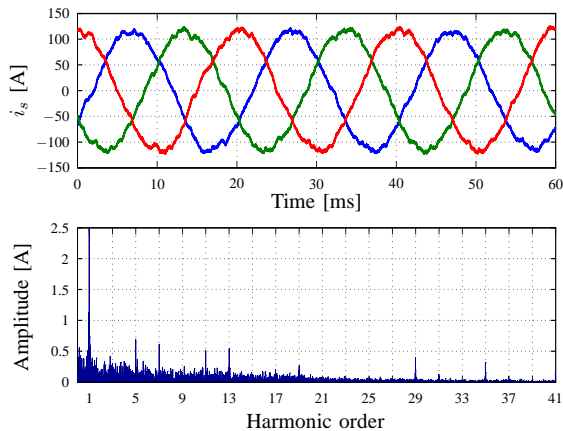
The per unit system is established using the base quantities $V_B = \sqrt{2/3}V_{\text{rat}} = 4899 \text{ V}$, $I_B = \sqrt{2}I_{\text{rat}} = 194 \text{ A}$ and $f_B = f_{\text{rat}} = 50 \text{ Hz}$. The induction machine is of the direct-on-line (DOL) type, featuring a very low leakage inductance. Parameters of the MV converter are listed in Table III. Stator voltage and current waveforms recorded in the experimental setup with the drive system controlled by MP³C are shown in Fig. 11 while the machine is operated at 50 Hz frequency and at partial load. The fundamental component of the stator voltages in Fig. 11(a) is shown only partially in the spectrum to emphasize the harmonic content. The rms phase amplitude is 3.49 kV, which corresponds to the rated phase-to-phase machine voltage of 6 kV. Higher-order voltage harmonics are shown in full detail in Fig. 11(a). It is evident that the discrete-order components are of negligible amplitude up to the 31st harmonic.

The current waveforms produced by MP³C are shown in Fig. 11(b). Also here, the fundamental component of the current (85 A rms) is shown only partially in the spectrum in order to focus on the very low amplitudes of the current harmonics. MP³C produces just 3.77% total demand distortion (TDD) referred to the rated current of the controlled machine (137 A). For comparison purposes, the respective voltage and current waveforms and harmonic spectra produced by direct torque control (DTC) are shown in Fig. 12. These waveforms were recorded at the same operating point and at the same switching frequency as in Fig. 11. In this case, DTC produces stator currents with 6.37% TDD.

The dynamic performance of MP³C was also tested in the experimental setup. The recorded electromagnetic torque of the electrical machine is shown in the upper trace of Fig. 13 where a step change from full-load to no-load operation takes place at $t \approx 6.5 \text{ ms}$. The machine torque settling time is less than 4 ms with very little undershoot. MP³C is able to maintain



(a) Three-phase stator voltage waveforms and harmonic spectrum; the rms amplitude of the phase voltage is 3.49 kV.



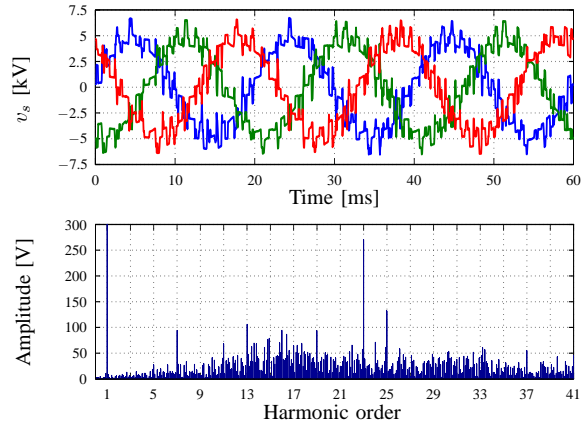
(b) Three-phase stator current waveforms and harmonic spectrum; the rms amplitude of the phase current is 85 A. MP³C produces 3.77% total demand distortion (TDD) referred to the rated current of the controlled machine (137 A).

Fig. 11. Experimental results produced by MP³C in steady-state operation ($f_1 = 50$ Hz and 62% machine current). Optimized pulse patterns of $d = 10$ switching instants per quarter-wave are employed.

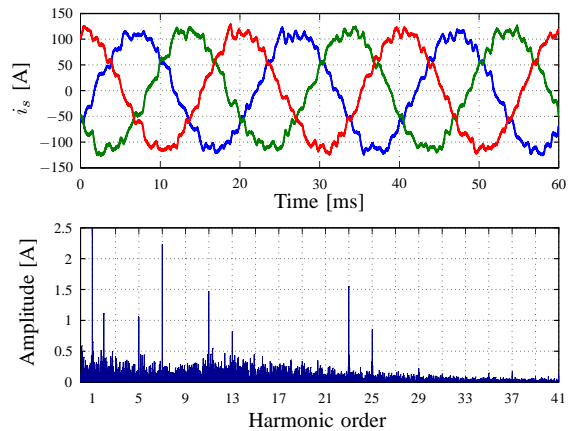
control of the machine even after the transient condition has elapsed, as validated by the current waveforms shown in the lower trace of Fig. 13.

VI. CONCLUSIONS

Industrial medium-voltage (MV) drives must meet stringent performance requirements with regard to the total demand distortion (TDD) of the currents in the windings of the controlled machine. This is a challenging task owing to the low switching frequencies in MV converters. The solution proposed in this paper, model predictive pulse pattern control (MP³C), is presented for use with a five-level active neutral point clamped MV drive. Optimized pulse patterns (OPPs) are calculated offline to generate minimum harmonic distortion of the currents under ideal conditions. The OPPs are modified in real-time by MP³C such that optimization of the stator flux trajectory is achieved. This optimization is performed in a pre-



(a) Three-phase stator voltage waveforms and harmonic spectrum; the rms amplitude of the phase voltage is 3.49 kV.

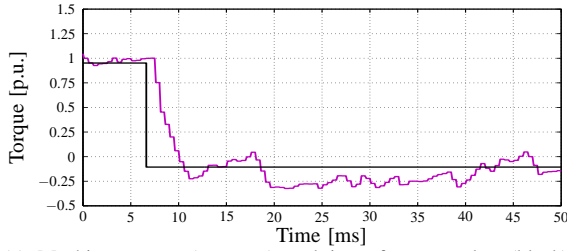


(b) Three-phase stator current waveforms and harmonic spectrum; the rms amplitude of the phase current is 85 A. DTC produces 6.37% total demand distortion (TDD) referred to the rated current of the controlled machine (137 A).

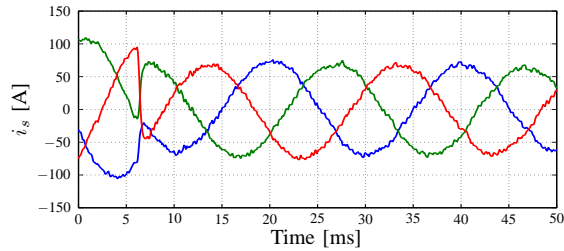
Fig. 12. Experimental results produced by DTC in steady-state operation ($f_1 = 50$ Hz and 62% machine current). The recorded waveforms are at the same switching frequency as in Fig. 11.

dictive manner: required future modifications of switching instants are calculated within an event-based prediction horizon. Control actions are evaluated in a computationally effective fashion: the minimum number of required switching instants is used to compensate errors in the stator flux trajectory. This enables the application of the proposed method to any control platform of any industrial drive.

MP³C compensates non-idealities of the drive system that deteriorate the steady-state performance of OPPs in real-world applications. The result is minimum TDD of the produced currents even in applications that employ direct-on-line (DOL) machines, which typically feature very low leakage inductances. The superior performance of MP³C was demonstrated in the laboratory with a test ANPC-5L drive operated at steady-state. The experimental setup was also subjected to step changes in the reference torque while the drive was operating at rated frequency. The large-signal response of the



(a) Machine torque (magenta) and its reference value (black). The torque quantities are given in p.u..



(b) Three phase stator currents during the transient process in (a).

Fig. 13. Experimental results of a step change of the torque reference at $t \approx 6.5$ ms. The drive is operated at $f_1 = 50$ Hz.

electromagnetic torque of the controlled machine validates the high dynamic performance provided by MP³C.

REFERENCES

- [1] F. Kieferndorf, M. Basler, L. A. Serpa, J.-H. Fabian, A. Coccia, and G. A. Scheuer, "A new medium voltage drive system based on ANPC-5L technology," in *Proc. IEEE Int. Conf. Ind. Technol.*, Viña del Mar, Chile, Mar. 2010, pp. 643–649.
- [2] P. Barbosa, P. Steimer, J. Steinke, L. Meysenc, M. Winkelkemper, and N. Celanovic, "Active neutral-point-clamped multilevel converters," in *Proc. IEEE Power Electron. Spec. Conf.*, Recife, Brazil, Jun. 2005, pp. 2296–2301.
- [3] F. Kieferndorf, P. Karamanakos, P. Bader, N. Oikonomou, and T. Geyer, "Model predictive control of the internal voltages of a five-level active neutral point clamped converter," in *Proc. IEEE Energy Convers. Congr. Expo.*, Raleigh, NC, Sep. 2012, pp. 1676–1683.
- [4] J. Holtz and N. Oikonomou, "Neutral point potential balancing algorithm at low modulation index for three-level inverter medium-voltage drives," *IEEE Trans. Ind. Appl.*, vol. 43, no. 3, pp. 761–768, May/Jun. 2007.
- [5] H. S. Patel and R. G. Hoft, "Generalized techniques of harmonic elimination and voltage control in thyristor inverters: Part I—Harmonic elimination," *IEEE Trans. Ind. Appl.*, vol. IA-9, no. 3, pp. 310–317, May 1973.
- [6] —, "Generalized techniques of harmonic elimination and voltage control in thyristor inverters: Part II—Voltage control techniques," *IEEE Trans. Ind. Appl.*, vol. IA-10, no. 5, pp. 666–673, Sep. 1974.
- [7] G. S. Buja and G. B. Indri, "Optimal pulsewidth modulation for feeding ac motors," *IEEE Trans. Ind. Appl.*, vol. IA-13, no. 1, pp. 38–44, Jan. 1977.
- [8] J. Holtz and N. Oikonomou, "Synchronous optimal pulsewidth modulation and stator flux trajectory control for medium-voltage drives," *IEEE Trans. Ind. Appl.*, vol. 43, no. 2, pp. 600–608, Mar./Apr. 2007.
- [9] —, "Estimation of the fundamental current in low-switching-frequency high dynamic medium voltage drives," *IEEE Trans. Ind. Appl.*, vol. 44, no. 5, pp. 1597–1605, Sep./Oct. 2008.
- [10] T. Geyer, N. Oikonomou, G. Papafotiou, and F. Kieferndorf, "Model predictive pulse pattern control," *IEEE Trans. Ind. Appl.*, vol. 48, no. 2, pp. 663–676, Mar./Apr. 2012.
- [11] J. B. Rawlings and D. Q. Mayne, *Model Predictive Control: Theory and Design*. Madison, WI: Nob Hill, 2009.
- [12] J. M. Maciejowski, *Predictive Control with Constraints*. Englewood Cliffs, NJ: Prentice-Hall, 2002.
- [13] P. Correa, M. Pacas, and J. Rodríguez, "A predictive torque control for inverter-fed induction machines," *IEEE Trans. Ind. Electron.*, vol. 54, no. 2, pp. 1073–1079, Apr. 2007.
- [14] P. Cortés, M. P. Kazmierkowski, R. M. Kennel, D. E. Quevedo, and J. Rodríguez, "Predictive control in power electronics and drives," *IEEE Trans. Ind. Electron.*, vol. 55, no. 12, pp. 4312–4324, Dec. 2008.
- [15] T. Geyer, G. Papafotiou, and M. Morari, "Model predictive direct torque control—Part I: Concept, algorithm and analysis," *IEEE Trans. Ind. Electron.*, vol. 56, no. 6, pp. 1894–1905, Jun. 2009.
- [16] T. Geyer, "Low complexity model predictive control in power electronics and power systems," Ph.D. dissertation, Autom. Control Lab. ETH, Zurich, 2005.
- [17] —, "Generalized model predictive direct torque control: Long prediction horizons and minimization of switching losses," in *Proc. IEEE Conf. Decis. Control*, Shanghai, China, Dec. 2009, pp. 6799–6804.
- [18] T. Geyer and S. Mastellone, "Model predictive direct torque control of a five-level ANPC converter drive system," *IEEE Trans. Ind. Appl.*, vol. 48, no. 5, pp. 1565–1575, Sep./Oct. 2012.
- [19] J. Holtz and J. Quan, "Drift and parameter compensated flux estimator for persistent zero stator frequency operation of sensorless controlled induction motors," *IEEE Trans. Ind. Appl.*, vol. 39, no. 4, pp. 1052–1060, Jul./Aug. 2003.
- [20] J. Holtz, "The representation of ac machine dynamics by complex signal flow graphs," *IEEE Trans. Ind. Electron.*, vol. 42, no. 3, pp. 263–271, Jun. 1995.
- [21] D. Luenberger, "An introduction to observers," *IEEE Trans. Automat. Contr.*, vol. 16, no. 6, pp. 596–602, Dec. 1971.